Computer Modeling and the Design of Optimal Underwater Imaging Systems

JULES S. JAFFE, ASSOCIATE MEMBER, IEEE

Abstract—**A computer model to simulate the formation of underwater images has been developed. The model incorporates the inherent and apparent properties of the propagation of light in water. In a treatment similar to that of McGlamery [10], an image is approximated as a linear superposition of several image components. The model has been used to simulate the relative advantages of different camera/light configurations. The results indicate that extremely large gains in image contrast can be obtained via careful design of beam patterns and the manipulation of camera and light locations. The performance of range-gated systems is explored, and it is demonstrated that these systems are presently power-limited. In order to obtain better quality images at larger distances, an imaging configuration is proposed which consists of scanning an incoherent light beam across the field of view of a camera. The incoherent light-scanning system is shown to have advantages over both conventional imaging techniques as well as range-gated methods.**

I. Introduction

THE VISIBILITY of underwater objects which have been illuminated by natural or artificial light has been of long-standing interest to investigators working in oceanographic environments. The extreme attenuating and scattering properties of water have limited underwater visibility in many situations where greater distance, contrast, or recognizability would be of advantage.

Pioneering work in underwater optics was accomplished in the 1950's and 1960's by Duntley [4]. The results of his research program, which was initiated at the Massachusetts Institute of Technology and then pursued at the Visibility Laboratory of the Scripps Institute of Oceanography, defined the basic limitations of underwater imaging. Further experiments in underwater imaging were performed at the Scripps Visibility Laboratory, as well as by other groups in the 1970's.

In this article we will examine the current status and limitations of underwater imaging. These limitations are due to both the environment and the currently available technology. In determining the limits for observing underwater images, there are two factors which must be taken into account: Contrast, and power. In a common situation, the main limitation to observing underwater images is not the lack of power which reaches the imaging system with information about an object; rather, it is a result of the amount of scatter due to the common volume of water intersected by the field of view of the camera and the illumination source. In this circumstance, the system is contrast-limited. In other situations, image contrast may be extremely high; however, the amount of power falling upon the receiving sensor is too small to be detectable. In this case the image is power-limited.

It is easy to see that the possibilities for long-range underwater imaging are quite limited. A simple "back-of-the-envelope" calculation can illustrate the point. Assume that one has a kilowatt of photons at 488 nm (2.45×10^{21}) and that the round-trip attenuation can be computed as

$$P(\text{reflected}) = P(\text{projected}) \exp(-2cr). \quad (1)$$

Here c is the total attenuation coefficient which is associated with the exponential decay of light per unit distance. The number of attenuation lengths which would be necessary in order to receive one photon can now be computed; the answer is approximately 50. Using typical values for attenuation of deep-ocean water, coastal water, and bay water as 0.05 m^{-1}, 0.2 m^{-1}, and 0.33 m^{-1}, visibility of only 500, 125, and 75 m is possible. This is clearly an over-estimate, which does not take into account the finite aperture of a camera, the reflectivity of an underwater object, and the spreading of a light beam on its way toward illuminating an underwater object. Obviously, the designer of underwater imaging systems lives in a world with limited possibility.

Recent advances in electronic image collection and processing continue to allow new schemes in ocean imaging to be feasible. One advance that affects the subject matter of this paper is the availability of inexpensive image-processing hardware. This permits the full display of the dynamic range of an imaging system. Small differences in grey levels can be enhanced in order to make them visible to the human observer. Another recent advance is in recording technology. Charge-Coupled Device (CCD) cameras have allowed imaging systems to approach the quantum-limited behavior of photons. The combination of these new technologies will certainly make the next generation of underwater imaging systems more effective and affordable.

The experiences of many decades of designing underwater imaging experiments can be summarized quite simply. The basic trade-offs in underwater imaging design are between camera-light separation, contrast, and power. Naturally, these are all functions of environmental conditions. A convenient metric for the performance of an underwater imaging system is the range in total attenuation lengths at which the system

Manuscript received December 22, 1988; revised October 31, 1989. This work was supported by a Grant from the Pew Memorial Foundation, by the Office of Naval Research under Contract No. N-00014-87-C-0795, and by the Naval Coastal Systems Center.

The author is with the Marine Physical Laboratory, A-005, Scripps Institution of Oceanography, University of California at San Diego, La Jolla, CA 92093.

IEEE Log Number 8933616.

0364-9059/90/0400-0101$01.00

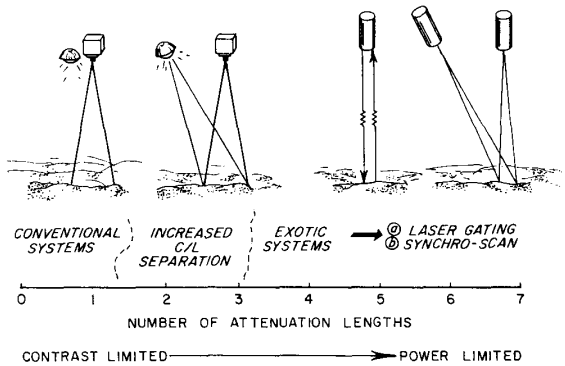

Fig. 1. A general guide to imaging system performance.

provides acceptable images. The most conventional systems using coincident positioning of camera and lights can usually image well at one attenuation length, but are contrast-limited at greater ranges. Systems which are based on increasing the separation between the camera and lights to distances obtainable on small submarines or underwater robots (ROV's) (3–5 m) can usually image at distances of up to 2–3 attenuation lengths, but then they also succumb to backscatter limitations. If performance greater than 3 attenuation lengths is desired, more exotic systems are necessary. Two examples which will be explored in this article are laser range-gated systems, and systems that employ scanning light beams. These more exotic lighting systems are usually power-limited. These concepts are illustrated in Fig. 1.

In order to explore the obtainable performance of underwater imaging systems, a computer model has been developed with sufficient flexibility to model a variety of situations. Based upon the predictions of the model, the utility of different imaging configurations can be evaluated. In this way, the ocean-imaging system designer can use the computer as a Computer-Aided Design (CAD) device in order to optimize the imaging system design.

The computer modeling system is concerned primarily with artificially lit scenes. An underwater imaging system is therefore constructed from components which include a lighting source, a reflectance map, and a camera. Using the computer model, it is possible to change the environmental parameters of the system for different simulations, and in this manner explore the effects of different environments upon system performance. It is also possible to explore the effects that different imaging geometries have upon the resultant imagery by varying the placement of camera and lights.

We have called this system of computer programs UNCLES, for UNderwater Camera Light Experiment System. Its routine use has greatly augmented our research program in underwater imaging. It has been used to predict the performance of a variety of underwater imaging systems, ranging from towed platforms to ROV's. One example is the ARGO vehicle of the Deep Submergence Laboratory of the Woods Hole Oceanographic Institution, which participated in the discovery of the *Titanic* [7].

In this article the physical theory is presented first, and then the mathematical implementation of the physics is described. Several examples of the output of the UNCLES system are used to illustrate the various trade-offs that are inherent in underwater-imaging system design. In one case, the model is used to illustrate the performance of a well-known underwater lighting configuration (LIBEC (Light-In-Back-of-the-Camera)) [11] and compare it with an alternate design. The alternate system is proposed in order to minimize the backscatter degradation which hinders the performance of the LIBEC design. It is demonstrated that the proposed configuration provides substantial advantages over the LIBEC system.

In addition, the UNCLES system has been used to explore more exotic imaging geometries. The predicted performance of a range-gated imaging system is examined. It is demonstrated that this system has excellent contrast but that it is power-limited. The current state-of-the-art in light generation and sensor technology thus limits the practical distances at which range-gated systems can be used.

In designing and using the UNCLES system, our main goal has been to formulate imaging configurations that would allow the acquisition of underwater images with greater range and contrast than is currently accessible. In pursuit of this, a technique is proposed for acquiring images that consists of scanning a striped beam of white light across the field of view. The technique has several advantages: Backscatter can be minimized, and the inherent power limitations of current laser technology can be overcome to some extent. As a result, it is predicted that lighting systems that are based upon this technology will yield better images at greater ranges than either the current generation of range-gated systems or more conventional techniques.

II. Physics

The groundwork for our basic understanding of the propagation of electromagnetic waves in dielectric media was formulated in the 19th century and is expressed via the Maxwell equations. Since light is a wave phenomena, it must obey the wave equation. This can be demonstrated by the straightforward manipulation of the Maxwell equations. In this article we will be concerned with the underwater propagation of electromagnetic waves in isotropic homogeneous media. Here, the two basic ways by which light interacts with matter are attenuation and scattering. The attenuation coefficient for pure water is predicted by the Maxwell equations to be related to the complex (imaginary) part of the complex index of refraction. Absorbtion can also occur due to pigmented species in the water. A simple definition of scattering is any divergence from a straight-line path. In the underwater realm, light can either be diffracted by particles whose dimensions are on the order of the wavelength of the light, or be refracted by particulate matter which has a different index of refraction than the media.

Empirically, these phenomena can be grouped together by measurement. As has been already mentioned, the total attenuation coefficient c is the decay constant associated with the removal of light intensity per unit distance:

$$E(r) = E(o)e^{-cr}. \tag{2}$$

Here r is the distance, and E is the irradiance at positions o

and r. The constant c can be further decomposed as a sum of two quantities, the absorbtion and scattering coefficients, so that

$$c = a + b$$

and

$$E(r) = E(o)e^{-ar}e^{-br}. \tag{3}$$

The above treatment is precisely the case for an infinitely small thin beam in which no radiation is scattered back into the beam. In this case, all scattering and absorbtion events lead to the loss of light flux. Transmissometers measure an approximate value of c by maintaining a very highly collimated and finely focused beam.

The total scattering coefficient b is the superposition of all scattering events at all angles. It is the integral of the volume scattering function $\beta(\theta)$ over all solid angles:

$$b = \int_0^{\pi} \beta(\theta)\, d\omega = 2\pi \int_0^{\pi} \beta(\theta) \sin\theta\, d\theta. \tag{4}$$

The four quantities a, b, c, and $\beta(\theta)$ represent the inherent properties of the medium. They are distinct from the apparent properties, as they do not depend upon the radiance field about a measurement point [12]. In principle, these quantities are all that are needed in order to predict the propagation of light underwater. This can be an extremely complicated problem if a, b, c, and $\beta(\theta)$ also depend on their location $\bar{r}$ in a three-dimensional ocean.

In observing optical quantities, one is limited to measuring either radiance or irradiance fields. Over the years, transmissometers, scattering meters, and cameras have been used in order to record underwater radiance fields [4], [9]. These measurements provide a data base for defining the parameters that are input into the computer modeling system.

As a final point we remark that one technique for predicting the underwater-radiance distribution consists of solving the equation for underwater-radiative transfer:

$$\frac{dL}{d\bar{r}}(\bar{r}, \theta, \varphi) = -cL(\bar{r}, \theta, \varphi) + L^*(\bar{r}, \theta, \varphi) \tag{5}$$

where

$$L^* = \iint \beta(\theta, \varphi; \theta', \varphi')L(\bar{r}, \theta', \varphi') \sin\theta'\, d\theta'\, d\varphi' \tag{6}$$

and L is the radiance distribution at position $\bar{r}$, and β is as defined above. Here L^* is the gain of radiance by scattering, and the term involving c is the loss due to attenuation. As this equation is, in general, difficult to solve, other techniques have evolved in order to predict radiance fields from the inherent optical properties and boundary conditions. The UNCLES computer system was designed for this purpose.

III. Image Modeling

A number of different approaches have been taken by different researchers in predicting the outcome of underwater-imaging experiments. A Navy handbook [5] contains a great deal of information based upon the results of Monte Carlo model studies. Its primary use is as an empirical guide in the fabrication of underwater-imaging systems. An alternate approach [2] uses a semianalytic Monte Carlo model which was adopted from scattering physics for underwater use. Another approach taken by Gordon and Knittel [6] is to formulate a set of analytic equations in order to take into account multiple scattering. Their results seem to agree well with the Monte Carlo simulations to a range of 6 attenuation lengths.

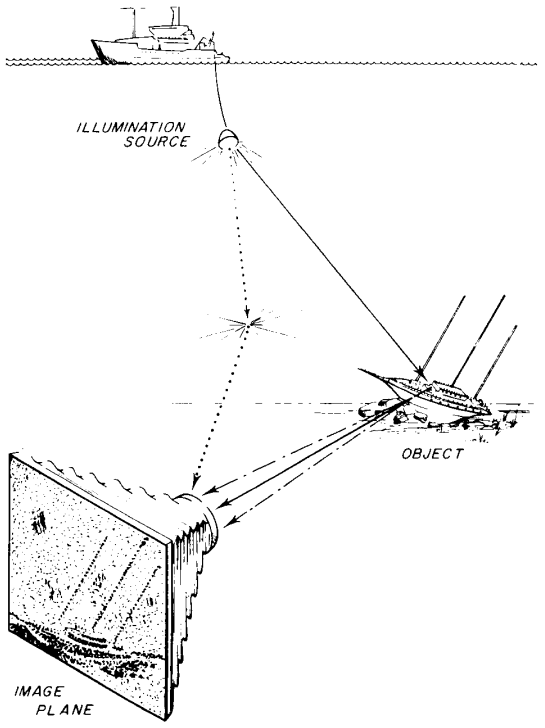

Fig. 2. Components of an underwater image. (——) = direct component. (— · —) = forward-scattered component. (· · · · ·) = backscattered component.

The approach presented here is closely related to a model formulated [10] at the Visibility Laboratory. The model can be described as a hybrid approach, in that linearization is incorporated in certain situations in order to simplify the computation. When this approximation cannot be made, the predicted radiance fields are calculated explicitly.

As illustrated in Fig. 2, an underwater-imaging experiment consists of tracing the progression of light from a light source to a camera. Several pathways exist by which the light can travel to the image plane of the camera. These pathways may or may not include light which has been reflected by an object. Therefore the light which has entered the camera may or may not have been reflected by the object. The light which enters the camera without reflection from the object gives rise to an imaging component which is called backscatter. Considering the light reflected by the object, or in this case a reflectance map, we can distinguish two components that are incident upon the camera plane: 1) Light which has not been scattered in the intervening water, called the direct component; and 2) light which has been small angle scattered, called the forward-scattered component. We choose to represent an im-

age as being the linear superposition of three components: a) Backscatter; b) forward scattering; and c) a direct component. These pathways are illustrated in Fig. 2. Mathematically,

$$E_T(\text{total}) = E_d(\text{direct}) + E_{fs}(\text{forward scatter}) + E_{bs}(\text{backscatter}). \quad (7)$$

A. The Direct and Forward-Scattered Component

In order to calculate the light reflected from the map, the irradiance pattern incident upon the reflectance map must first be calculated. The origin of this irradiance is the light source, considered here to be a point-source characterized by a beam pattern $\text{BP}(\theta_s, \varphi_s)$, a function of polar angles θ_s and φ_s. The units of $\text{BP}(\theta_s, \varphi_s)$ are in W/m^2, where $\text{BP}(\theta_s, \varphi_s)$ is the irradiance on a hemispherical shell at a distance of 1 m from the light source. In order to calculate the irradiance incident upon the map, this beam pattern is attenuated and spherically spread. The irradiance incident upon the reflectance map can then be calculated as

$$E_I'(x', y', \theta_s, \varphi_s) = \text{BP}(\theta_s, \varphi_s)\cos\gamma\frac{e^{-cR_s}}{R_s^2}. \quad (8)$$

Here x', y' refer to the fixed coordinate system with respect to the planar reflectance map located at $z' = 0$; $R_s(x_s', y_s', z_s', x', y', 0)$ is the distance 1 m from the source to a point on the reflectance map; γ is the angle between a perpendicular to the reflectance map at a given x', y' location and a line between the x', y' location and the source; and the constant c is the total attenuation coefficient. The geometry is illustrated in Fig. 3. Note that the primed coordinate system is associated with the reflectance map, and the unprimed coordinate system is associated with the camera plane. A more accurate representation of the incident irradiance E_I takes into account the spreading of illumination due to the small-angle forward-scattered component as well as adding back in a contribution due to small-angle forward scattering. An approximate value can be found by a convolution with a point-spread function g, as is typical in image processing [14]. In this case,

$$E_I(x', y', 0) = E_I'(x', y', 0) * g(x', y'|R_s, G, c, B) + E_I'(x', y', 0) \quad (9)$$

where

$$g(x', y'|R_s, G, c, B) = \{\exp(-GR_s) - \exp(-cR_s)\}F^{-1}\exp(-BR_sf) \quad (10)$$

and G is an empirical constant ($|G| \leq c$). The operator F^{-1} indicates that an inverse Fourier transform is taken of a function of B, which is an empirical damping factor, and f, which is a radial frequency in cycles/rd. Note that the "$*$" operator denotes convolution. Wells [15] has shown that in the small-angle scattering approximation, the linear relationship of (9) is valid. This is equivalent to the formulation proposed by McGlamery [10]. It is also justifiable on a more theoretical basis, as is considered in the treatment in [6]. In [6], the relationship was found to agree with Monte Carlo calculations for distances of up to 6 attenuation lengths.

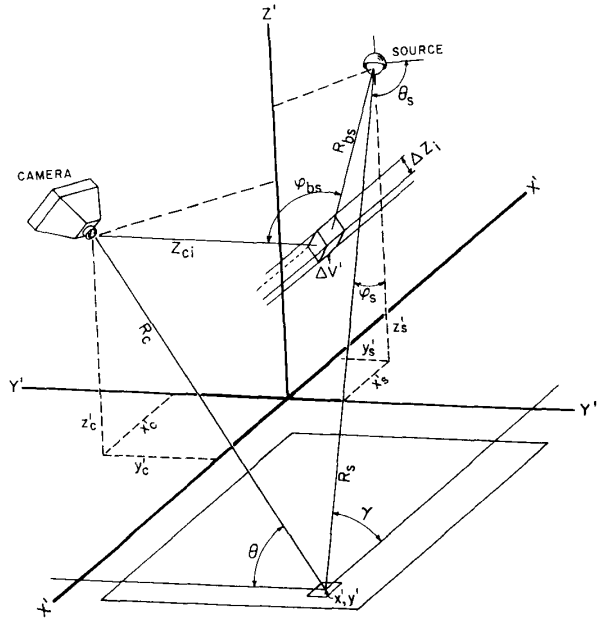

Fig. 3. The coordinate system used for the computer model.

Now in order to compute the reflected radiance, the values of the incident irradiance pattern are multiplied by the reflectance values of the reflectance map. In the UNCLES system an object is represented by a planar reflectance map $M(x', y')$ located in three-dimensional space at a fixed orientation. Note that $M(x', y') \leq 1$. Typical values for objects of oceanographic interest are $0.02 \leq M(x', y') \leq 0.1$ [3]. In addition, a geometric factor of $\cos\theta$ is taken into consideration in accordance with Lambert's law. The angle θ is the angle between the reflectance map and a line between the position x', y' and the camera aperture, as illustrated in Fig. 3.

In order to predict the irradiance incident upon the image plane of the camera, it is necessary to consider the geometric optics of the camera, the attenuation of the medium between the reflectance map and the camera, and the spherical spreading of the reflected wave. Taking these factors into consideration, the irradiance incident upon the image plane of the camera can be represented as

$$E_d(x, y) = E_I(x', y', 0)\exp(-cR_c)\frac{M(x', y')}{4f_n} \cdot \cos^4\theta T_l\left[\frac{R_c - F_l}{R_c}\right]^2 \quad (11)$$

where R_c is the distance from an x', y' position on the reflectance map to the camera, f_n is the f number of the camera of focal length F_l, and T_l is the transmittance of the lens.

The forward-scattered component can then be calculated from the direct component via the convolution relationship,

$$E_{fs}(x, y) = E_d(x, y, o) * g(x, y|R_c, G, c, B) \quad (12)$$

where g is represented by (10).

B. The Backscatter Component

The calculation of the backscatter component is the most computationally intense part of the computer program. This is because the linear approximation is no longer valid as the backscattered light enters the camera from a large distribution of angles. Alternatively stated, the small-angle approximation used in making the linear approximation in computing the forward-scattered component is no longer valid.

The approach taken in this work follows that of McGlamery [10] in that three-dimensional space is sliced into planes of thickness Δz_i that are parallel to the image plane of the camera. The irradiance incident upon each of these planes is then calculated, as above, by computing the direct component and then adding an additional amount of irradiance due to the light that is small angle scattered.

The next step in computing the backscatter component is to determine the resulting image due to each of these illuminated slabs. The irradiance incident upon the aperture of the camera is a superposition of these illuminated volume elements weighted by the value of the volume-scattering function. By representing the irradiance in three-dimensional space propagating away from the light source as $E_s(x', y', z')$ and following the above arguments, the irradiance incident on the volume elements can be viewed as a superposition of a direct and forward-scattered component:

$$E_s(x', y', z') = E_{s,d}(x', y', z') + E_{s,fs}(x', y', z') \quad (13)$$

$$E_{s,d}(x', y', z') = \mathrm{BP}(\theta, \varphi)\frac{\exp(-cR_{bs})}{R_{bs}^2} \quad (14)$$

$$E_{s,fs}(x', y', z') = E_{s,d}(x', y', z') * g(x', y', z'|R_{bs}, G, c, B). \quad (15)$$

Now taking a weighted superposition of the intensities from a given slice, we can compute the radiant intensity which is scattered toward the camera element x, y due to volume $\Delta V'$:

$$H_{bs}(\varphi, x, y) = \beta(\varphi_{bs})E_s(x', y', z')\Delta V' \quad (16)$$

where $\beta(\varphi)$ represents the volume-scattering function; $\Delta V'$ is an incremental volume in three-dimensional space; and the angle φ_{bs} is the angle between a line from the volume under consideration to the light source and a line from the volume to the camera. Next, the image of this volume of water must be calculated. In this case, following arguments similar to those above, the direct component of this backscattered irradiance $E_{bs,d}(x, y)$ can be represented [10] as

$$E_{bs,d}(x, y) = \sum_{i=1}^{N} \exp(-cZ_{ci})\beta(\varphi_{bs})E_s(x', y', z') \cdot \frac{\pi \Delta Z_i}{4f_n^2}\cos^3\theta T_l\left[\frac{Z_{ci} - f_l}{Z_{ci}}\right]^2. \quad (17)$$

Here ΔZ_i is the thickness of the backscattering volume $\Delta V'$; and Z_{ci} is the distance from a point in the camera to the center of the backscatter slab. The value N extends from $i = 1$ for the first backscatter plane, to N for the plane adjacent to the target. As was noted previously, the total irradiance due to the backscattered image $E_{bs}(x, y)$ can then be calculated by adding an additional forward-scattered component:

$$E_{bs}(x, y) = E_{bs,d}(x, y) + E_{bs,d}(x, y) * g(x, y|R_c, G, c, B). \quad (18)$$

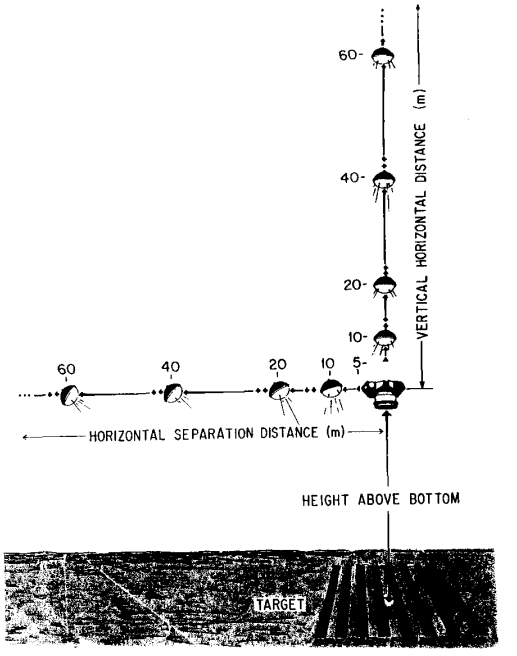

Fig. 4. The geometry used to compare side lighting and LIBEC.

IV. Computer Simulations

In the previous sections the mathematical formulation of the UNCLES system has been described. In this section we demonstrate results obtained by computer simulations. The goal of the simulations was to evaluate the relative merits of different types of imaging system configurations.

Initially, we consider the problem of placing camera and lights in different positions in order to explore the relative advantages of several different systems. One of these configurations places the camera and light source in vertical displacement, while the other places the camera and lights in horizontal displacement. The geometry is illustrated in Fig. 4. Here it is illustrated that the LIBEC configuration [11] consists of placing the light source directly above the camera. One way of achieving this configuration for towed vehicle configurations is by locating the light source above the platform on the towing cable.

The performance of this system is compared to an alternate proposal which places the light source to the side of the camera. As illustrated in Fig. 4, the side-lighting configuration places the light source on the same vertical level as the camera; however, it is separated from it horizontally.

In these simulations the camera has been positioned directly above a bar-pattern reflectance map at altitudes of 20, 40, and 60 m in very clear ($c^{-1} = 20$ m) ocean water. The separation distance between the camera and the light source was then

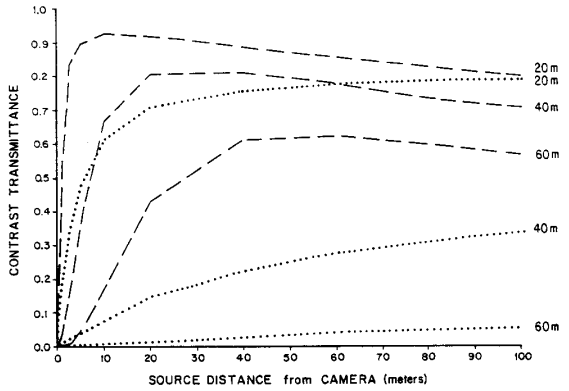

Fig. 5. Contrast transmittance versus separation for the two systems. (· · · · ·) = LIBEC light source. (— — —) = side-mounted light source.

systematically varied for both the LIBEC and side-lit case, and the resultant images were computed.

The results of the computer simulations are summarized in Fig. 5, which depicts a graph of the contrast transmittance at a central location in the image versus the separation between the camera and light source. The contrast transmittance $C_t(x, y)$ is defined as the fraction of the direct component in the image at a location x, y:

$$C_t(x, y) = \frac{E_d(x, y)}{E_T(x, y)}. \tag{19}$$

It is clear from the contrast transmittance plot that the use of side lighting greatly improves performance. Although this knowledge has been part of the folklore of the underwater imaging trade, this study provides hard evidence for this opinion. Moreover, it would be very difficult to predict that such large gains could be made for small increments in the horizontal separation. An inspection of Fig. 5 reveals that for the intermediate altitude of 40 m, an increase in separation of 3 to 5 m results in an approximate doubling of the image contrast. The results also reveal that the side-lighting system at a 40-m altitude will perform better than the LIBEC system at a 20-m altitude.

The LIBEC system does maintain a substantial advantage over the situation where the camera and lights are co-located. Presumably, the reason that the LIBEC system achieves better performance is because the area directly in front of the camera is not illuminated as intensely as in the co-location case.

An obvious difference between the two situations is the difficulty of experimentally achieving the side-lighting geometry. Although quite large separations can be achieved vertically by using a tow-cable geometry, this configuration has limited visibility capabilities. On the other hand, conventional vehicles can be 3–5 m in length [7]. If larger camera-light separation distances are desired, various possibilities exist in order to extend the separation distance between the camera and light source. Among these options are the following: Towing a light source, or lengthening the vehicle after deployment.

V. Advanced Imaging System: Range-Gated Performance

If a greater degree of imaging-system performance is desired for practical purposes, the underwater imaging-system designer can exploit a multitude of other options. These options involve utilizing more-complex hardware than do the imaging system designs considered above. Based upon either environmental or operational considerations, these more exotic imaging configurations may offer an increased level of performance which justifies the additional expense involved in their construction and operation.

In this section the performance of a specific implementation of a range-gated imaging system is explored. Range-gating a light source and receiver has been suggested as a method which decreases the relative content of backscatter in underwater images [8]. The method consists of propagating a pulse of light of short duration into the medium. In this way, only a slab of water of finite thickness is illuminated. If the receiving device is timed to be open for a time duration equal to that of the light pulse, then by varying the onset time of the device, the collection of information about only a thickness of water at a given range will be allowed. Furthermore, if the distance of an object within the field of view is known, the camera can be activated so that almost all of the reflected illumination and none of the backscatter will enter the camera. The idea has already been illustrated in Fig. 1.

In order to explore the advantages and disadvantages associated with range-gated imaging, the UNCLES program has been used to simulate the performance of a range-gated imaging configuration. In this article we consider the result of creating a short pulse of light of length δt, reflecting this from a test target, and then imaging the reflected illumination with a range-gated receiver. The camera and illumination source were located together. The algorithm used computed both the direct and forward-scattered components as detailed above. The difference in this case is that only a subset of the illuminated slabs of water is allowed to contribute to the backscatter component. The range of distances of these slabs was calculated so that backscattered light from the first slab would reach the camera at the same time as the light from the leading edge of the pulse that had been directly reflected. The last slab was located at the reflectance map.

Various options are possible that utilize the principle of range-gating. In this section, the results of two different simulations are compared. In one simulation, a blue green laser with a pulse duration of 17 ns was simulated. In another, the performance of a gated strobe of white light with a pulse duration of 35 ns was simulated. In both cases it was assumed that the receiving device could be opened for an exactly equivalent amount of time.

An example of an image from the range-gated simulations is shown in Fig. 6. For the case shown in the illustration, the inverse attenuation coefficient c^{-1} of the water was assumed to be 6.6 m, and the altitude of the device was 28 m. The image is for a pulse length of 17 ns. The figure illustrates the large degree of image contrast which is possible in range-gated imagery.

In order to determine the actual values that would be recorded by a camera, conversion from the UNCLES output values derived from the previous equations is necessary. Fig. 7 illustrates the illumination power levels at the receiver, integrated over 1 s, due to both a blue-green laser and gated

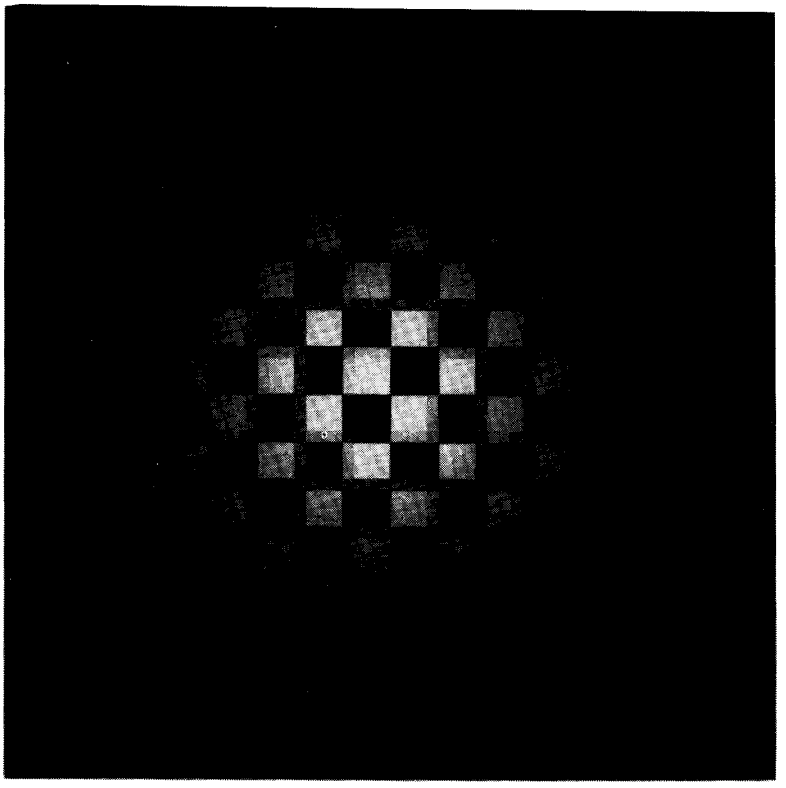

Fig. 6. Simulation of the appearance of a range-gated image.

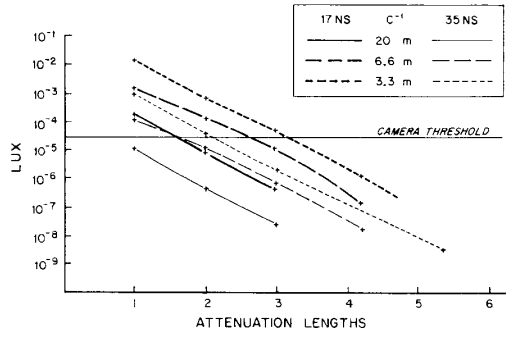

Fig. 7. Predicted power levels for the range-gated systems considered.

strobe. A conversion formula has been used to convert, from the output of the UNCLES program M_c, the value for a 1 W lighting source:

$$E_c = M_c * P_s * N_s * N_w * N_r. \tag{20}$$

Here E_c is the output value in lx at a given x, y position in the camera plane; P_s is the amount of power which is output by the illumination device; N_s is the photometric conversion output for the illumination source; N_w is the water radiant efficiency transfer (the range-dependent attenuation of the different parts of the spectrum) [5]; and N_r is the efficiency of the reflector (useful for strobe illumination only). Although the UNCLES model has yet to be calibrated absolutely for the real world, it is assumed here that the results will be valid at least for comparative studies.

For the blue-green laser, a pulse repetition rate of 25 pulses/s was assumed. In this case, a value of 500 W/lm for N_s was used. N_w was assumed to be unity, and P_s was computed for a 35 MJ/pulse laser over a period of time equal to 1 s. This is equivalent to integrating the response of the camera over 1 s, or 25 pulses of the laser at 35 MJ/pulse. Note that commercially available lasers meet these specifications. The graph also depicts a threshold level for an ample signal to be recorded by a video camera. Typical values for both SIT cameras and slow readout CCD devices are 5×10^{-5} lx [13]. Note that these are the most sensitive cameras that are available.

The irradiance levels at the camera that would be due to a gated strobe lamp with an integration time of 35 ns were also computed. It is assumed that the spectrum of the light source is identical to that of a thallium iodide lamp with a power of 250 W. Here, a conversion factor of 85 lm/W was used for N_s to convert from radiometric to photometric values. Also, in this case, because the water does not pass all bands of the broad spectrum of the light equally, N_w must be determined. This is an empirical factor which is a range-dependent, environment-dependent efficiency factor. Standard values of these coefficients are itemized in a Navy Handbook [5]. In order to compute the value for P_s, the duty cycle for a gated repetitive strobe needs to be incorporated in the integrated illumination-intensity calculation. The duty cycle for

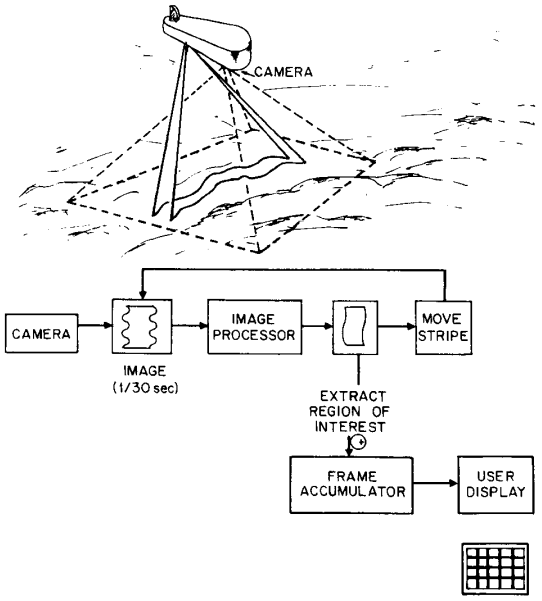

Fig. 8. Flowchart for the proposed stripe scanning system.

a strobe-light repeating illumination with a pulse length of 35 ns every 4 μs would be 0.009. These values are commensurate with using a gated CID camera.[1] The main disadvantage of incoherent gated illumination, in this respect, is that the gating results in extremely inefficient use of the illumination.

On the basis of the computer simulations it appears that range-gated imaging will have excellent contrast values, but limited performance due to the power limitations. As can be seen from the graph of Fig. 7, the laser range-gated system is limited to a performance of one attenuation length in clear water ($c^{-1} = 20$ m), and only two attenuation lengths in cloudier conditions. The performance demonstrated by the strobe system is even worse. The performance obtainable with this system is not even one attenuation length for the clear water situation, and is less than one to two attenuation lengths for poorer conditions.

Based on the above set of simulations for both conventional imaging systems and range-gated techniques, it seemed of interest to formulate an imaging methodology which would allow images to be acquired at greater ranges with adequate contrast. In the case of the conventional techniques, the main limitation to imaging performance is contrast. On the other hand, in the case of the range-gated technique, the main limitation is illumination power. In the next section, an idea is detailed which uses conventional lighting sources and allows the acquisition of images with adequate contrast at longer ranges.

VI. Scanned White-Light Stripe Performance

In this section a technique will be considered which consists of scanning a stripe of incoherent light across the field of view of a camera. The situation is illustrated in Fig. 8. In this simulation the source and receiver are separated on a vehicle with a length of 5 m. As already discussed, increasing the distance between the source and receiver can lead to better images by reducing the common backscatter volume between the lighting source and camera. The configuration proposed in this section is an extension of that technique. The basic idea consists of scanning an extremely narrow beam along the axis which joins the camera and light source, digitally recording a sequence of images, and using image-processing techniques in order to dissect out the high contrast components and synthesize an image which consists of a superposition of the individual pictures.

Upon illumination, the image of a single stripe can be recorded on the camera. In this example we have assumed an exposure time of 1/30 of a second because it corresponds to one video frame collection time. The image can be digitized, or "grabbed," by an image processor in 1/30 of a second. Once the image is in the digital memory of the image processor, an edge detection algorithm is used to detect the boundary of the illuminating stripe. In this case a simple derivative trigger was used to signal the onset of the stripe. Knowing the width of the narrow, collimated, striped beam and the approximate height of the vehicle, a region of interest is then delineated for each single image. This area of interest is then added to the contents of another frame buffer. The current generation of image-processing computers permit the feedback of digitized images into an accumulator at video rates.

This process is then repeated for the next scanned line, after moving the beam by 1/15 of the field of view, and continues for the number of individually scanned lines in the picture. In this way, the image is divided into 15 individual sections that are then added together. The final image viewed consists of a superposition of all of these individual striped images.

[1] Xybion Model ISG-01 Gated Intensified Solid-State (CID) Video Camera. Xybion Electronic Syst. Corp., 7750-A Convoy Court, San Diego CA.

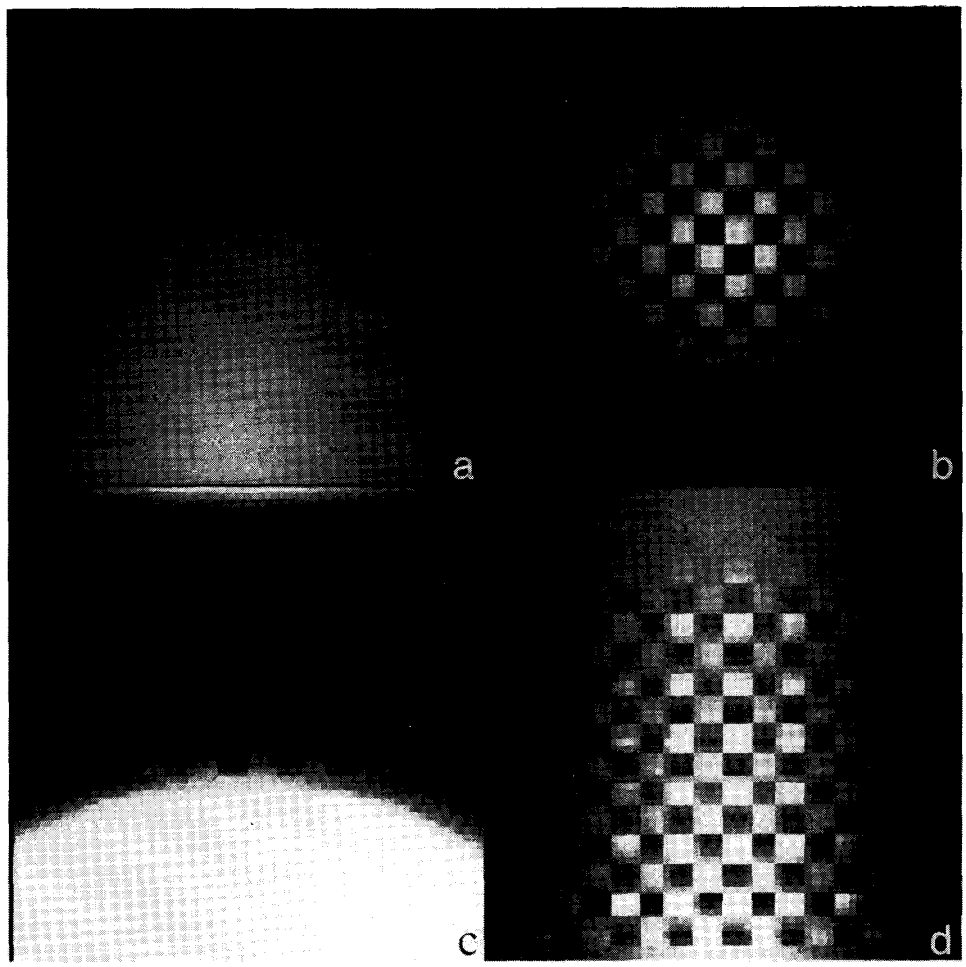

Fig. 9. (a) The total component of an image collected at 16.5 m; $c = 0.3$ m. (b) The direct component for the same geometry as in (a). (c) An individual image collected with the stripe scanning system. (d) An example of the composite image collected with the stripe scanning system.

Finally, contrast-enhancement procedures can be used in order to increase the visibility of such a device, providing that the receiving sensor has the available dynamic range. Fig. 8 illustrates a flow chart for the entire system procedure.

The result of using an extended version of the UNCLES program to calculate the performance of an imaging system is shown in Fig. 9. A camera light separation of 5 m was used in this example. Fig. 9(a) depicts the image which would be collected by a conventional imaging system at a range of 16.5 m in $c^{-1} = 3.3$-m water (5 attenuation lengths). Obviously, no image contrast is visible. Fig. 9(b) contains the image of just the direct component of the image in Fig. 9(a). As a reminder, the direct component is the light which is backscattered from the target without being scattered in the intervening water between the target and camera. This image represents the best obtainable performance that can be achieved. Fig. 9(c) depicts one of the 15 striped images that were added together in order to obtain the final synthesized image depicted in Fig. 9(d).

Fig. 9(d) is the final simulated image for the striped illumination system. It should be compared with Fig. 9(b). As evidenced, the striped illumination system provides images at greater ranges than are possible with conventional imaging. Here, the image of a test target of a checkerboard pattern is clearly visible in the synthesized image. As can be seen, the contrast in the image is quite adequate for observer recognition of important features. It is also predicted that, based on the camera sensitivity and the power of available thalium iodide lights (250 W were used here), the image will be detectable by a CCD camera.

The processing which was applied to each of the individual images was to use a simple derivative trigger to signal the onset of the stripe. The trigger value was estimated in the following way: First, the average value of the picture parallel to the stripe was estimated for each row of the image. Next, a value was determined for a threshold which was half-way between the minimum and maximum values of the row averages. Then this threshold was used to decide the onset of the region of interest for each of the individual 15 images. As was mentioned, knowing the width of the stripe and the approximate vehicle height, the termination of the region of interest for each of the 15 images could be determined.

Only the regions of interest for the 15 images were then

added together. This produced a composite image which was better than the conventional picture in Fig. 9(a), but there were still gradations in image intensity, mostly parallel to the stripe orientation. To equalize the grey-level distribution in neighboring rows an equalization algorithm was used. The algorithm consisted of choosing one row as a template. Next, each of the rows was linearly transformed by adding a constant and then multiplying by a constant (for each row), which minimized the mean squared difference in the grey level between each pixel in the row and the template value in the corresponding column location. This produced a final image (depicted in Fig. 9(d)) which had much less grey-level variation than the original image. More sophisticated processing algorithms were not explored because it was felt that the visibility of objects would be quite good for this final result.

VII. Conclusions

In this article we have documented the theory and performance of a system of computer programs to simulate the appearance of underwater objects as seen by underwater cameras. The UNCLES system permits the underwater-lighting system designer to vary the locations of cameras, lights, and a reflectance map as a function of the environmental parameters. The system incorporates the inherent properties of the underwater medium such as attenuation, scattering, and the volume-scattering function in order to simulate image formation. The model has permitted the routine design of underwater-imaging systems as a computer-aided design (CAD) tool.

The results of the computer model have been illustrated by comparing the performance of a well-known lighting configuration (LIBEC) with that of an alternate proposed system. The alternate system incorporates side lighting as a preferred method of illuminating a target without creating as much backscatter. Therefore, the side-lighting system provides superior performance.

The improved performance of the side-lit configuration is illustrated by comparing the contrast in the images for various altitudes. The relative increase in the contrast as a function of separation distance is extremely steep for the side-lighting system as compared to the LIBEC approach. In addition, the side-lighting system is more efficient in its use of lighting power. It therefore makes sense to utilize side lighting where possible in order to increase performance.

Simulations have also been performed for other, more exotic imaging configurations. The cases that have been compared are a range-gated system, and a system based on a new idea of imaging a scanned beam of white light, in conjunction with image-processing techniques.

Although laser range-gating demonstrates superior performance in image constrast, it is concluded that the power limitations of the current generation of lasers prevent long-range image observation. The case of a single-gated laser with a pulse length equal to 17 ns and a repetition frequency equal to 25 pulse/s, with a power level equal to 35 MJ/pulse, has been examined. In this case we estimate that two attenuation lengths of visibility are available in typical coastal or bay waters, and one attenuation length is possible in extremely clear ocean water.

The situation of using a gated, incoherently pulsed lighting source has also been examined. Here, a 250-W strobe with a pulse length equal to 35 ns and a repetition rate of 4 μs has been simulated. In this case, one needs to consider the passband characteristics of the water. The illumination levels for this configuration are, in fact, smaller than those of the gated laser owing principally to the limited duty cycle of the device. As a result, the possibilities for long-range illumination are even worse than for the above laser simulations.

The methodology for using range-gated techniques which has been presented in this paper is not the only one possible. In fact, alternate techniques that use large receiving apertures would hold an advantage over the system considered here. These systems have the potential to image at greater ranges because they collect more reflected light via a larger aperture [3]. An unfortunate aspect of these systems is the complexity of their required hardware.

A technique which involves scanning a striped beam of illumination has also been proposed. The idea takes advantage of the reduced common backscatter volume which results when camera and lights are separated. The predicted performance of such systems is shown to allow underwater viewing to 5 attenuation lengths in cloudy conditions. Since the use of striped illumination for underwater imaging relies primarily upon camera-light separation, it may not be possible to take advantage of this technique on a vehicle of limited size. In this case, the range-gating alternative may be preferred.

Further advantages of the scanning light system exist. A common technique in three-dimensional vision systems is to use structured lighting in order to obtain a three-dimensional map of a given scene [1]. The geometry suggested here for the light stripe system could take advantage of the relationship between stripe displacement and altitude in order to obtain microbathymetry. Automated edge detection could thus be used in order to produce a topographical map. It is concluded that structured lighting holds many advantages in underwater optical system performance. It is hoped that future underwater imaging systems will take advantage of some of the techniques elaborated above in order to extend our abilities to see underwater.

Acknowledgment

The author would like to thank many people for contributing to the progress of this work over the years. B. McGlamery of the SIO Visibility Laboratory and J. Riley and Y. Agarwal of the Woods Hole Oceanographic Institution provided an early version of the UNCLES program. C. Dunn performed most of the computer programming.

References

[1] D. H. Ballard and D. M. Brown, *Computer Vision*. Englewood Cliffs, NJ: Prentice-Hall, 1982.
[2] F. Chilton, D. D. Jones, and W. K. Talley, "Imaging properties by the sea," *J. Opt. Soc. Amer.*, vol. 59, no. 8, 1969.
[3] T. H. Dixon, T. J. Piviritto, R. F. Chapman, and R. C. Tyce, "A range-gated laser system for ocean floor imaging," *MTS J.*, vol. 17, no. 4, 1983.
[4] S. Q. Duntley, "Light in the sea," *J. Opt. Soc. Amer.*, vol. 53, 1963.
[5] C. J. Funk, S. B. Bryant, and P. J. Heckman Jr., *Handbook of Underwater Imaging System Design*, Ocean Techn. Dept., Naval Undersea Ctr., San Diego, CA, July 1972.
[6] A. Gordon and M. R. Knittel, "Underwater multiple scattering of light for system designers," NUC, Techn. Paper 371, 1973.
[7] S. E. Harris and R. D. Ballard, "ARGO: Capabilities and deep ocean

explorations," in *Proc. Oceans '86* (Washington, DC), Sept. 23–25, 1986, pp. 6–8.
[8] P. Heckman and R. T. Hodgson, "Underwater optical range gating," *IEEE J. Quantum Elec.*, vol. QE-3, no. 11, 1967.
[9] N. G. Jerlov, *Marine Optics* (Elvesier Oceanog. Series No. 14). New York: Elvesier, 1976.
[10] B. J. McGlamery, "A computer model for underwater camera systems," in *Ocean Optics VI*, S. Q. Duntley, Ed., *SPIE*, vol. 28, 1979.
[11] R. B. Patterson, "Backscatter reduction for artificially illuminated in-water camera systems," *Opt. Eng.*, vol. 14, no. 4, 1975.
[12] R. W. Preisendorfer, *Hydrologic Optics*, vol. II: Foundations. Honolulu, HI: U.S. Dept. of Commerce, 1976.
[13] *RCA Electro-Optics Handbook*, RCA, Solid-State Div., Electro-Optics and Devices, Lancaster, PA, 1974.
[14] A. Rosenfeld and A. Kak, *Digital Picture Processing*. New York: Academic, 1982.
[15] W. H. Wells, "Loss of resolution in water as a result of multiple small-angle scattering," *J. Opt. Soc. Amer.*, vol. 59, 1969.

Jules S. Jaffe (A'85) received the B.A. degree from the State University of New York at Buffalo in physics in 1973, the M.S. degree in biomedical information science from the Georgia Institute of Technology, Atlanta, in 1974, and the Ph.D. degree in biophysics from the University of California, Berkeley, in 1982.

After spending several years working in industry as an Image-Processing Consultant, he joined the Woods Hole Oceanographic Institution as a Pew Memorial Fellow in 1984 at the Assistant Scientist level, and was promoted to Associate Scientist in 1988. He is currently an Assistant Research Oceanographer at the Scripps Institution of Oceanography, Marine Physical Laboratory, University of California at San Diego, which he joined in 1988. His research interests are in the areas of image reconstruction and restoration, with a special emphasis on three-dimensional systems. He is currently designing underwater optical and sonar imaging systems for ocean exploration.